Biochimica et Biophysica Acta 1847 (2015) 212–222

Contents lists available at ScienceDirect

Biochimica et Biophysica Acta

journal homepage: www.elsevier.com/locate/bbabio

Electron-transfer kinetics in cyanobacterial cells: Methyl viologen is a poor inhibitor of linear electron flow

Pierre Sétif *

iBiTec-S, CNRS UMR 8221, CEA Saclay, 91191 Gif-sur-Yvette, France

ARTICLE INFO

Article history:
Received 18 September 2014
Received in revised form 24 October 2014
Accepted 28 October 2014
Available online 1 November 2014

Keywords:
Paraquat
NADP photoreduction
P700 photooxidation kinetics
Photosystem I
Ferredoxin
Ferredoxin-NADP$^+$-oxidoreductase

ABSTRACT

The inhibitor methyl viologen (MV) has been widely used in photosynthesis to study oxidative stress. Its effects on electron transfer kinetics in *Synechocystis* sp. PCC6803 cells were studied to characterize its electron-accepting properties. For the first hundreds of flashes following MV addition at submillimolar concentrations, the kinetics of NADPH formation were hardly modified (less than 15% decrease in signal amplitude) with a significant signal decrease only observed after more flashes or continuous illumination. The dependence of the P700 photooxidation kinetics on the MV concentration exhibited a saturation effect at 0.3 mM MV, a concentration which inhibits the recombination reactions in photosystem I. The kinetics of NADPH formation and decay under continuous light with MV at 0.3 mM showed that MV induces the oxidation of the NADP pool in darkness and that the yield of linear electron transfer decreased by only 50% after 1.5–2 photosystem-I turnovers. The unexpectedly poor efficiency of MV in inhibiting NADPH formation was corroborated by *in vitro* flash-induced absorption experiments with purified photosystem-I, ferredoxin and ferredoxin-NADP$^+$-oxidoreductase. These experiments showed that the second-order rate constants of MV reduction are 20 to 40-fold smaller than the competing rate constants involved in reduction of ferredoxin and ferredoxin-NADP$^+$-oxidoreductase. The present study shows that MV, which accepts electrons *in vivo* both at the level of photosystem-I and ferredoxin, can be used at submillimolar concentrations to inhibit recombination reactions in photosystem-I with only a moderate decrease in the efficiency of fast reactions involved in linear electron transfer and possibly cyclic electron transfer.

1. Introduction

Inhibitors of electron flow have been widely used for the characterization of electron/proton transfer reactions in photosynthesis [1]. The herbicide methyl viologen (MV; also named paraquat) is thought to inhibit photosynthetic electron flow by accepting electrons from photosystem I (PSI) [2]. It is highly water-soluble and exhibits a low midpoint potential of −446 mV *vs* NHE [3]. After single reduction from the divalent to the monovalent cation state, MV is rapidly reoxidized by oxygen [4], a reaction that leads to superoxide production, with subsequent formation of other deleterious ROS species [5]. The ability of MV to induce oxidative stress has been extensively used to study the physiological adaptation of photosynthetic organisms and to study/select mutants resistant or sensitive to this stress (cyanobacteria: [6–15]; plants: [16–19]). Despite this, the MV reduction process is very poorly characterized *in vivo*, regarding both its exact site(s) of action and its kinetic properties.

During linear electron transfer (LET), NADP$^+$ is reduced into NADPH. This involves light-induced charge separation within PSI which, besides the oxidation of the primary donor P700, eventually leads to the fast (sub)microsecond reduction of the terminal electron acceptor (F_A, F_B) [20,21], a pair of closely spaced [4Fe–4S] clusters [22,23]. The different steps following PSI charge separation and leading to NADP$^+$ reduction have been studied *in vitro* [24–27] whereas only NADPH formation has been observed *in vivo* up to now [28,29] (see however [30]). These steps involve the fast microsecond reduction of the soluble acceptor ferredoxin (Fd) by PSI followed by NADPH formation by ferredoxin-NADP$^+$-oxidoreductase (FNR). This enzyme catalyzes the two electron reduction of NADP$^+$ using two reduced ferredoxins (Fd_{red}). In the cyanobacterium *Synechocystis* sp. PCC 6803 (hereafter named *Synechocystis*) as in many cyanobacteria, two FNR isoforms are present [31]. Under phototrophic conditions, the large isoform FNR_L, which is bound to the phycobilisome, constitutes the most part of FNR [32]. The short isoform FNR_S is similar to plastidial FNR and is expressed under growth conditions involving respiratory electron transfer [32]. Purified FNR_S and FNR_L (bound to a phycobilisome subcomplex) have been previously found to exhibit rather similar catalytic properties [33]. Apart from LET, PSI is

Abbreviations: CBc, Calvin–Benson cycle; CET, cyclic electron transfer; DCMU, the photosystem II inhibitor 3-(3,4-dichlorophenyl)-1,1-dimethylurea; ET, electron transfer; (F_A, F_B), terminal PSI acceptor; (F_A, F_B)$^-$, singly reduced terminal PSI acceptor; Fd, ferredoxin; Fd_{red}, reduced ferredoxin; FNR, ferredoxin-NADP$^+$-oxidoreductase; FNR_{ox}, oxidized FNR; FNR_{sq}, singly reduced FNR or semi-quinone form; FNR_L, large FNR isoform; FNR_S, small FNR isoform; LET, linear electron transfer; MV, methyl viologen; OPPc, oxidative pentose phosphate cycle; PSI, photosystem I

* Tel.: +33 169089867.
E-mail address: pierre.setif@cea.fr.

http://dx.doi.org/10.1016/j.bbabio.2014.10.008
0005-2728/

also involved both in cyclic electron transfer (CET) and recombination reactions. The contribution of these two processes is expected to increase relatively to LET when the pool of stromal reductants (PSI acceptors, Fd, NADP) is highly reduced.

The main goal of the present work was to show that MV can be used as a relatively specific inhibitor of PSI recombination reactions in cyanobacterial cells of *Synechocystis*. For this purpose we studied *in vivo* both NADPH formation and decay and $P700^+$ kinetics. We also studied by flash-absorption spectroscopy the effect of MV addition in reconstituted systems comprising PSI, PS/Fd and PSI/Fd/FNR to tentatively correlate the *in vitro* electron transfer (ET) kinetics to the *in vivo* observations. This led us to identify the sites of MV reduction and to quantify the rates of this process both *in vivo* and *in vitro*.

2. Materials and methods

2.1. Biological materials

In vitro experiments were performed with PSI monomers from *Synechocystis* [34] and recombinant forms of Fd [35] and FNR_S [27] from the same organism. The PSI, Fd and FNR_S concentrations were estimated by assuming absorption coefficients of 7.7 mM^{-1} cm^{-1} for $P700^+$ at 800 nm [27], 9.7 mM^{-1} cm^{-1} at 422 nm [36] and 9.0 mM^{-1} cm^{-1} at 461 nm [33], respectively. Wild type cells of *Synechocystis* were grown photoautotrophically as described in [29]. In cell suspensions, the chlorophyll *a* concentrations were measured after methanol extraction using the absorption coefficient given in [37] and the PSI concentrations were calculated by assuming an *in vivo* chlorophyll to P700 ratio of 105, in accordance with an estimated PSI/PSII ratio larger than 4 [29].

2.2. In vitro flash-absorption spectroscopy

Measurements were made at 22 °C under aerobic conditions (open cuvettes) as described previously [25,27] in the presence or absence of MV with PSI alone, with PSI + Fd and with PSI + Fd + FNR_S. A short laser flash was used for saturating PSI photochemistry. The laser excitation (wavelength, 695 nm; duration, 6 ns; energy, 30 mJ; one flash every 10 s for data averaging) was provided by a dye laser (Continuum, Excel Technology France) pumped by a Nd:YAG laser that was frequency-doubled (Quantel, France). Measurements were made either in 1-cm square cuvettes or in 1-mm cuvettes (1.2 mm pathlength) in 20 mM Tricine, pH 8.0, in the presence of 30 mM NaCl, 5 mM $MgCl_2$, 0.03% β-dodecyl maltoside, 2 mM sodium ascorbate and 25 μM 2,6-dichlorophenolindophenol. Measurements were made at 3 different wavelengths, 480, 580 and 800 nm. The PSI concentrations were calculated from $P700^+$ measurements at 800 nm (data not shown). Fd reduction by PSI was observed at 480 and 580 nm, two wavelengths at which this process was already studied [25,26], and where chlorophyll absorption is not too large, thus making relatively easy to avoid the actinic effects of the measuring light. The reoxidation of $(F_A, F_B)^-$ by MV was measured at 480 nm and the signals were compared to those measured in the presence of Fd. Absorption changes in the presence of FNR_S were studied at 580 nm, a wavelength at which formation of the FNR semiquinone gives a strong contribution [24].

2.3. In vivo $P700^+$ photooxidation kinetics

$P700^+$ photooxidation kinetics were measured at 32 °C in the infra-red region with a PAM spectrophotometer (Walz, Effeltrich, Germany) [38] which was modified for synchronization of data acquisition and shutter-controlled actinic light. The infra-red measuring light was modulated at 100 kHz. Samples were illuminated for 5 s with actinic far-red light from a halogen lamp which was filtered by 2 RG-695 long-pass filters (Schott, Germany) and heat-absorbing filters eliminating infra-red light. The sample was continuously stirred in an opened 1-cm cuvette except during the measurements. Cells were incubated in darkness at 32 °C for 8 min before addition of 20 μM DCMU. For all samples, two measurements ($\Delta t = 2$ min) with DCMU were averaged after 3 min of dark incubation before the first addition of MV.

For the study of $P700^+$ kinetics as a function of MV concentration, MV was added sequentially and the sample was incubated for 15 min after each addition before the measurement. Two control experiments were made to check that the increase in the rate of $P700^+$ formation with [MV] (Fig. 4A/B) cannot be attributed to an increasing incubation time at 32 °C: firstly, a sample with a single addition of 15 μM MV was initially studied after 15 min of dark incubation and this measurement was repeated after 30, 45 and 60 min of incubation, giving identical kinetics for all times; secondly, a sample with a single addition of 0.5 mM MV was studied after 15 min of dark incubation and gave the same kinetics as those of Fig. 4 with the same MV concentration (cumulative time of incubation of 75 min after the initial addition of 7.5 μM MV). For the study of $P700^+$ kinetics as a function of incubation time following the addition of 0.25 mM MV (Fig. 4C), a control experiment was made to check that the increase in the rate of $P700^+$ formation with the incubation time was not dependent upon the number of illuminations given to the sample before the measurement: in the control sample, a single measurement was made after 12 min of incubation following the addition of 0.25 mM MV with kinetics identical to those observed for a sample which had been measured 3 more times (after 3, 6 and 9 min of incubation).

2.4. In vivo NADPH measurements

Light-induced measurements were performed on *Synechocystis* cell suspensions at 32 °C as described in [29] using the NADPH/9-AA module [39] of a DUAL-PAM spectrophotometer (Walz, Effeltrich, Germany) in square 1 × 1 cm opened cuvettes. As described in [29], the fluorescence levels could be converted into NADPH concentrations by measuring the fluorescence signal of a known concentration of exogenous NADPH that was added to the cell suspension at the end of the experiment. It was also previously found that the light-induced NADPH concentrations thus calculated are 2- to 4-fold overestimated due presumably to enhancement of *in vivo* fluorescence compared to that of exogenous NADPH. Therefore these light-induced concentrations are qualified as "apparent concentrations" whereas the real light-induced concentrations are 2- to 4-fold smaller than the apparent ones. All baselines before illumination were set arbitrarily to 0.

3. Results

3.1. In vitro MV reduction by the reduced PSI terminal acceptor and by reduced Fd

Fig. 1 compares the reduction of 50 μM MV by PSI (trace b) and PSI/Fd (trace d) at 480 nm measured by flash-absorption spectroscopy. Control measurements were made in the absence of MV with identical PSI concentrations either in the absence (trace a) or presence (trace c) of Fd. The fast absorbance increases (not time-resolved) observed at time 0 in traces a and b reflect both the photooxidation of the PSI primary donor P700 and the single reduction of the PSI terminal acceptor (F_A, F_B). At 480 nm, P700 oxidation leads to an absorbance increase whereas (F_A, F_B) reduction corresponds to an absorbance decrease. The resulting signal is positive as the contribution of P700 is larger than that of (F_A, F_B) [25]. In the sample containing only PSI (trace a), only a small decay is observable on a 10 ms timescale, which is attributed to the slow recombination reaction between $P700^+$ and $(F_A, F_B)^-$ ($t_{1/2} \approx 80$ ms in PSI from *Synechocystis*, [40]). In trace b, the absorbance increase is attributed to the oxidation of $(F_A, F_B)^-$ by MV [25,41].

When Fd is added to PSI (trace c), the initial rise is followed by an absorbance decrease due to reduction of Fd by $(F_A, F_B)^-$, as previously observed [25] and in line with the observation that reduction of the

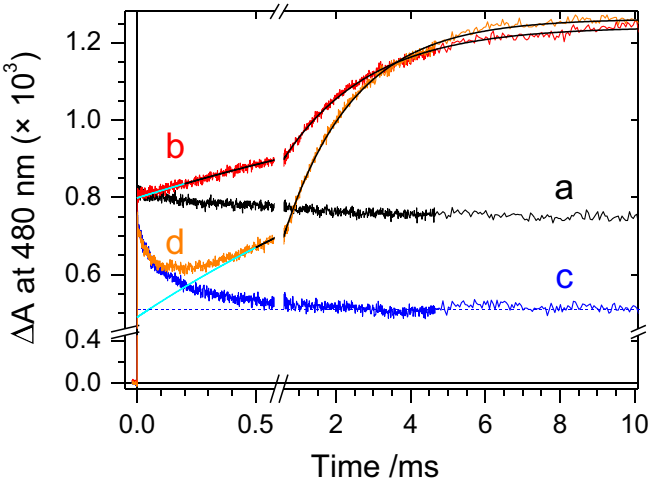

Fig. 1. *In vitro* MV reduction by the PSI terminal acceptor and by ferredoxin. Flash-induced absorption changes were measured at 480 nm in four different 1-cm cuvettes containing the same amount of PSI (0.19 μM), without (a and b) or with 1.0 μM Fd (c and d), and without (a and c) or with 50 μM MV (b and d). Traces with MV were fitted by equation: $y = y_0 + y_1 \times \exp(-kt)$ from 0.2 to 10 ms and from 0.5 to 10 ms for b and d, respectively. The fitting curves are shown in black. b: $y_0 = 1.24 \times 10^{-3}$, $y_1 = -0.44 \times 10^{-3}$, $k = 433\ s^{-1}$. d: $y_0 = 1.26 \times 10^{-3}$, $y_1 = -0.77 \times 10^{-3}$; $k = 532\ s^{-1}$. The fits were extrapolated to time 0 (in cyan). Experimental conditions: Tricine 20 mM pH 8, 30 mM NaCl, 5 mM $MgCl_2$. Each trace is an average of 16 measurements (Dt = 5 s).

[2Fe–2S] cluster of Fd gives a larger bleaching at wavelengths above 460 nm than reduction of the [4Fe–4S] PSI electron acceptor [26]. The concentration of Fd is well above the dissociation constant K_d of the PSI/Fd complex (measured to be 0.25 μM with the PSI preparation used in the present work [35]) so that ≈80% of Fd reduction occurs by first-order ET kinetics within a complex that is preformed before flash excitation. These kinetics have been already studied in detail and were found to be multiphasic with the presence of 3 first-order phases in the 0.5, 10 and 100 μs range [26]. Moreover it was shown in this study that the slowest phase is dominating at 480 nm, as observed here. A slower and minor phase of Fd reduction by a diffusion-limited second order process is also present at longer times.

When MV is added in the presence of Fd in a 50-fold excess, the kinetics are not modified up to 80 μs after the flash and an absorption increase appears only after this delay. This increases ends up at the same final signal level as that observed in the absence of Fd (b and d), in line with the expectation that the same final state is present in both cases (no reduced species left, only $P700^+$ is present at 10 ms). One can note that MV should not significantly contribute to the absorbance changes, as its reoxidation by oxygen ($k = 7.7 \times 10^8\ M^{-1}\ s^{-1}$ giving a $t_{1/2}$ of *c.* 4 μs with 250 μM of dissolved oxygen [4]), is much faster than its reduction.

Both absorbance rises with MV were fitted with a single exponential (smooth black traces). When extrapolated to time zero (cyan), the rising exponential with Fd/MV starts from the same signal level as that observed after full reduction of Fd (horizontal blue dotted line). This indicates that the most part of the rise can be ascribed to reoxidation of Fd_{red} by MV, although a minor part of it may be due to direct ET from $(F_A, F_B)^-$ to MV in PSI with no bound Fd. The interpretation that most of the rise is due to Fd_{red} reoxidation is corroborated by the observation that the rising rate is faster by *c.* 20% in the presence of Fd (see rates in Figure legend), which also indicates that Fd_{red} reacts with MV somewhat faster than $(F_A, F_B)^-$. It can be also noted that the dissociation rate of Fd_{red} from PSI was previously estimated to be between 800 and 3200 s^{-1} [27,36,42]. The fact that trace d deviates from c after 80 μs after the flash can be explained by this fast dissociation process. The present experiment was made with a 50-fold excess of MV over Fd. A control experiment was made with [MV] = [Fd] (= 1 μM). In this case, the kinetics with both acceptors present are superimposable to those with Fd alone (trace c) up to 5 ms (data not shown). In the following paragraph, reoxidation of $(F_A, F_B)^-$ by MV will be studied at different MV concentrations.

3.2. Rate constant of in vitro MV reduction by $(F_A, F_B)^-$

Measurements similar to those above were performed in the absence of Fd at different MV concentrations and are shown in Fig. 2A after subtraction of the control measurement without MV (≈ b–a of Fig. 1). This allows the large initial signal due to ($P700^+ - (F_A, F_B)^-$) formation to be eliminated. Moreover the slow drift due to $P700^+$ decay without MV was also subtracted from the signal so that the absorbance increases reflect only $(F_A, F_B)^-$ oxidation by MV. The rates of the absorption changes increase with the MV concentration (50 to 400 μM) and these changes can be well fitted by monoexponential rises (black curves). When plotted as a function of [MV], the fitted rates k_{obs} exhibit a linear dependence (Fig. 2B), from which a second-order rate of $8.8 \times 10^6\ M^{-1}\ s^{-1}$ is obtained. This rate is *c.* 40 times smaller than the second-order rate of Fd reduction by PSI measured under similar conditions [43] (*c.* $3.5 \pm 1.5 \times 10^8\ M^{-1}\ s^{-1}$, Table 1).

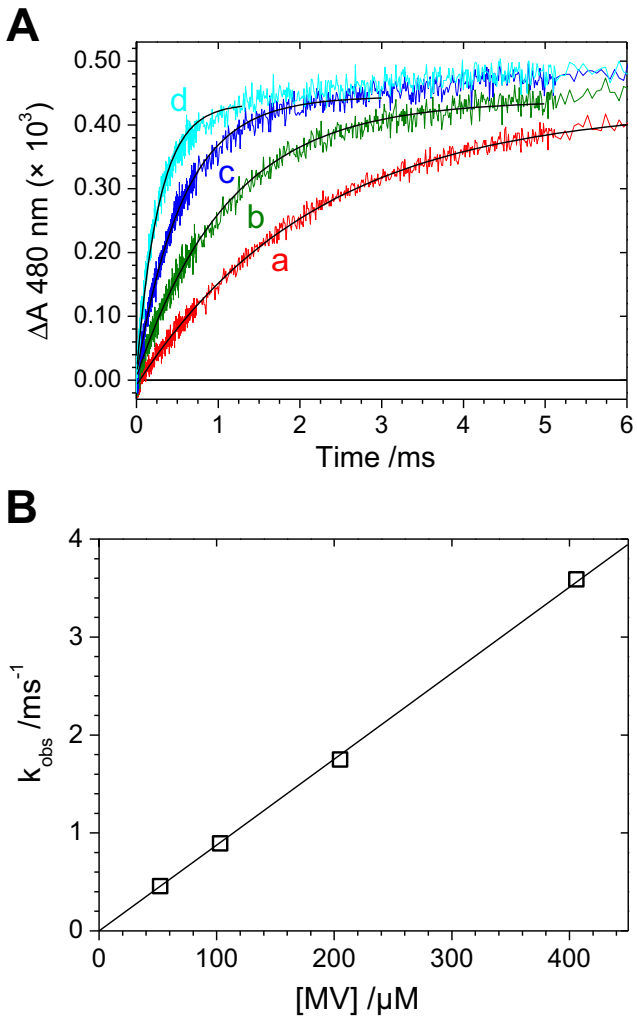

Fig. 2. *In vitro* MV reduction by the PSI terminal acceptor. Experiments in the absence of Fd were made under similar conditions as those of Fig. 1 (1-cm cuvettes, [PSI] = 0.18 μM) by plotting the signal difference between the signal recorded in the presence of MV (sequential additions) and that in its absence (such as (b–a) of Fig. 1). A. The cuvette with MV contained 52, 103, 205 and 406 μM mV (traces a to d). Difference kinetics were fitted with a monoexponential rising function $y = y_0 + y_1 \times \exp(-k_{obs}\ t)$ (black lines). B. The rates k_{obs} obtained from the fits were plotted as a function of MV concentration. The data points were linearly fitted by regression through the origin, giving a slope of $8.8 \times 10^6\ M^{-1}\ s^{-1}$.

Table 1
Second-order ET rate constants measured *in vitro* involving reduced stromal proteins and either MV or protein partners. The rate constants are given in $\mu M^{-1}\ s^{-1}$. Experimental conditions: Tricine 20 mM pH 8, 10 mM NaCl, 5 mM $MgCl_2$. Note that the rate constants given here for FNR were measured in the absence of $NADP^+$. Values may be 20% smaller for rate constants involving FNR–$NADP^+$ complexes as found in the case of FNR_{Sox} [27].

	PSI with $(F_A, F_B)^-$	Fd_{red}	FNR_{Ssq}
Rate constant with MV	8.8	11.8	0.53
Protein partner	Fd_{ox}	FNR_{Sox}	Fd_{red} [a]
Rate constant with partner	350 [b]	417 [c] FNR_{Lox}-PC[e] 238 [f]	400 [d]
Ratio of rate constants: protein partner/MV	40	20–36 [g]	750

[a] In contrast to the 2 other columns, the partner of FNR_{Ssq} is a reduced protein, in line with FNR_{Ssq} being an intermediate species which is reduced a second time during NADPH formation.
[b] From [43].
[c] The value given in [27] was reevaluated according to a better estimation of the FNR absorption coefficient [33].
[d] This was not measured precisely but estimated in [27] to be close to the value measured for FNR_{Sox} reduction by Fd_{red}.
[e] FNR_L-phycocyanin hexamer complex purified from *Synechocystis*. This complex is mimicking the *in vivo* situation where FNR_L is bound to the phycobilisome [33].
[f] The rate was previously measured under high salt conditions necessary for complex stabilization [33]. The present rate constant was calculated from the value measured with FNR_{Sox} under the present salt conditions (=417 $\mu M^{-1}\ s^{-1}$) and the ratio of rate constants measured in [33] in high salt for FNR_{Lox}-PC and FNR_{Sox} (=0.57).
[g] Values of 20 and 36 for FNR_{Lox}-PC and FNR_{Sox}, respectively.

3.3. *In vitro* MV reduction by Fd_{red} and singly reduced FNR_S

Data of Figs. 1 and 2 were obtained in 1 cm cuvettes, for which only submicromolar concentrations of PSI can be used because of its strong absorbance. In these experiments, we were also using a *c.* 5-fold excess of Fd over PSI. By contrast, data in Fig. 3 were obtained at 580 nm in 1-mm cuvettes with a 25-fold larger PSI concentration (≈5 μM) and with only a small excess of Fd over PSI (7 μM), in parallel with the relative stoichiometries observed in cyanobacterial cells ([Fd]/[PSI] ≈ 1.1 ± 0.25, [44]). FNR reduction was also studied by adding a 4-fold excess of FNR_S over PSI (20 μM *vs* 5 μM), and therefore over flash-induced Fd_{red}, in order to favor single reduction of FNR to its semiquinone form FNR_{sq} [27]. This species can be easily observed by its absorption at 580 nm [24], hence the choice of this wavelength for these measurements. In part A, kinetic traces are shown in the absence of MV either with PSI alone (trace a), PSI and Fd (trace b), PSI, Fd and FNR_S (trace c). Contrary to the positive signal at 480 nm (Fig. 1), the initial fast signal due to charge separation with PSI alone (trace a) is negative at 580 nm. This change in sign is due to the dominant contribution of the ($P700^+$–P700) which is positive at 480 nm and negative at 580 nm. With Fd (trace b), the relative contributions of the three first-order phases of Fd reduction are different at the 2 wavelengths, with the 100 μs phase being of minor amplitude at 580 nm [26] (see trace b in part B). With Fd and FNR (trace c), the signal increase is attributed to FNR_{sq} formation resulting from reduction of FNR_{ox} by Fd_{red}, a process that has been previously studied by flash-absorption spectroscopy through the same electron transfer cascade PSI/Fd/FNR [27]. The rate of FNR_{sq} formation (half of the final [FNR_{sq}] formed at 600 μs after the flash) is in line with previous observations [27] and may be attributed to a rate-limiting step such as PSI:Fd_{red} complex dissociation and/or reorganization of an ET-unproductive Fd_{red}:FNR_{ox} precomplex.

Part B shows the effect of increasing MV concentrations in the sample containing PSI and Fd (traces b to g; [MV] = 0/10/20/50/100 μM). Comparison of traces b and d shows that when MV is only in slight excess over Fd (10 *vs* 7 μM), the absorbance decrease due to Fd reduction is almost not modified but is followed by a slow absorbance increase which is attributed to Fd_{red} oxidation by MV. The rate of Fd_{red} reoxidation increases with the MV concentration and the corresponding

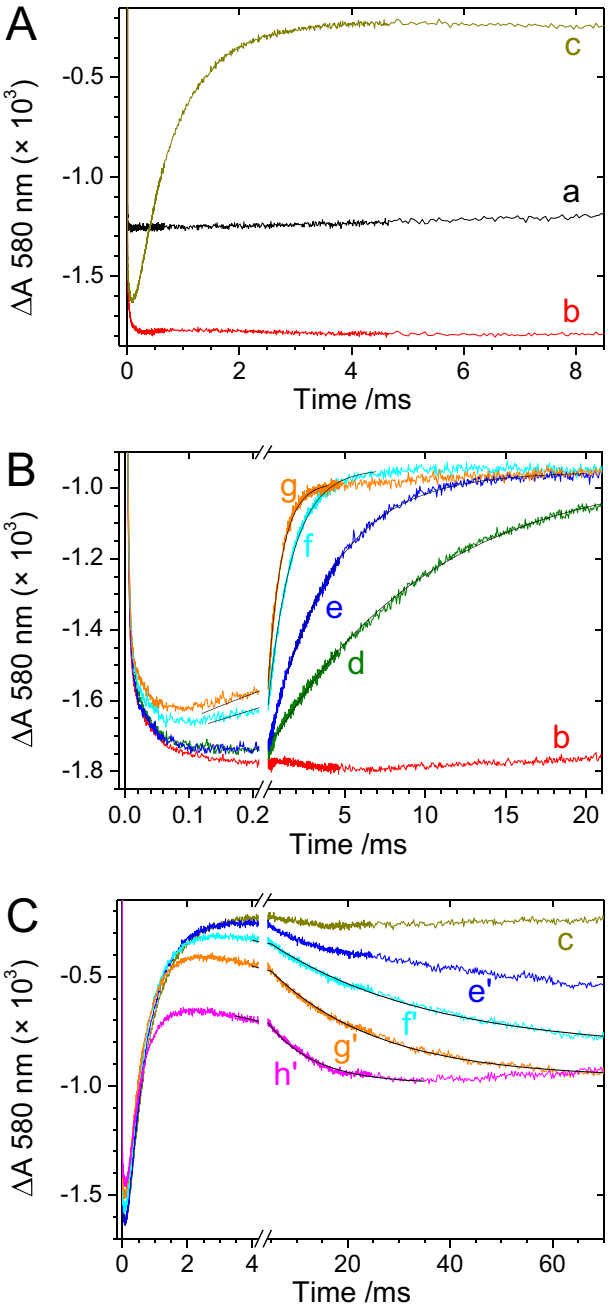

Fig. 3. *In vitro* MV reduction by ferredoxin and singly reduced FNR. Flash-induced absorption changes were measured at 580 nm in three different 1-mm cuvettes containing the same amount of PSI (5.12 μM) under similar pH and salt conditions as those of Fig. 1. Cuvette 1 contained only PSI (trace a), cuvette 2 contained also 7.0 μM Fd (traces b and d–g), and cuvette 3 contained 7.0 μM Fd and 20 μM FNR_S (traces c and e′–h′). MV was sequentially added to cuvettes 2 and 3. A. no MV; a, b and c were measured with PSI, PSI/Fd and PSI/Fd/FNR, respectively. B. PSI + Fd; b, d, e, f and g correspond to MV concentrations of 0, 10, 20, 50 and 100 μM, respectively. C. PSI + Fd + FNR; c, e′, f′, g′ and h′ correspond to MV concentrations of 0, 20, 50, 100 and 200 μM, respectively. Note that the time scales are different for the three parts of the Figure and that, in B and C, the same color and the same letter (primed or not) are used for identical MV concentrations.

k_{obs} resulting from fits with monoexponential rise functions (black curves) depend linearly upon it (Fig. SI1A in Supporting information). From this linear dependence, a second-order rate constant of 1.18 ± 0.04 × $10^7\ M^{-1}\ s^{-1}$ was calculated. This value is somewhat smaller than what was measured for spinach Fd (4 × $10^7\ M^{-1}\ s^{-1}$, [45]), a ferredoxin with a midpoint potential slightly lower than that of *Synechocystis* Fd (−426 mV *vs* −412 mV; [45] and [46], respectively). The presently observed rate of MV reduction by Fd_{red} is 30% larger

than the rate constant of MV reduction by $(F_A, F_B)^-$. It is also 28–36 times smaller than the second-order rate constant of FNR_{Sox} reduction (in the presence or absence of $NADP^+$) by Fd_{red} that was previously measured [27] (Table 1) so that it can be expected that MV competes poorly with FNR_{ox} for the reoxidation of Fd_{red}. This can be checked by adding FNR_S in the absence or presence of MV, as described in the next paragraph. It can be noted that for traces f and g (50 and 100 mM MV), the kinetics deviate significantly from those in the absence of MV as soon as 15 μs after the flash, contrary to what was observed at 480 nm (Fig. 1). However extrapolation of the rising kinetics to time zero gives a level of Fd reduction close to that in the absence of MV. We have no explanation for differences between 480 and 580 nm for MV effects in the presence of Fd.

Part C shows the effect of increasing MV concentrations in the sample containing PSI, Fd and FNR_S (c, e′ to h′; [MV] = 0/20/50/100/200 μM). In the absence of MV, FNR_{sq} is relatively long-lived as it can be inferred from the absence of decay up to 70 ms (trace c). In the presence of MV, the signal decay at t >4 ms is attributed to FNR_{sq} oxidation (e′–h′). Several features of this decay are noteworthy: firstly, for [MV] = [FNR] (=20 μM, trace e′), the decay is sufficiently slow that the maximum amount of FNR_{sq} is identical to its value without MV (c and e′ at 4 ms after the flash); secondly, for the highest MV concentrations (traces g′ and h′), the signal level after decay completion is identical to the final level measured with MV in part B (traces e–g). This remaining signal ($\Delta A \approx -0.95 \times 10^{-3}$) is attributed to $P700^+$ formation (*vs* P700 for the baseline), in line with all acceptors being eventually reoxidized after ET to MV; thirdly, the 3 fastest decays (traces f′–h′) could be well fitted by a monoexponential decay (black curves), and the deduced k_{obs} depend linearly on the MV concentration (see Fig. SI1B in Supporting information). From this linear dependence, an apparent second-order rate constant k_{2app} of $0.53 \pm 0.03 \times 10^6\ M^{-1}\ s^{-1}$ was calculated. This rate constant is qualified as apparent as FNR_{sq} oxidation may be a complex process involving, at least partially, Fd_{red} formation from FNR_{sq} followed by MV reduction by Fd_{red}. The rate constant k_{2app} is several orders of magnitude smaller than the second-order rate constant of FNR_{Ssq} reduction by Fd_{red}, which was found to be close to that of FNR_{ox} reduction by Fd_{red} [27] (Table 1). We may therefore anticipate that under similar concentrations of MV and FNR, the FNR-dependent NADPH photoproduction will not be much affected *in vivo* by the presence of MV. Such a prediction will be tested below by *in vivo* measurements of NADPH photoreduction (Section 3.5).

3.4. MV titration of the in vivo kinetics of PSI photooxidation

The kinetics of P700 photooxidation by continuous light were measured in suspensions of *Synechocystis* cells with a PAM spectrophotometer [38]. To ensure that PSII activity does not contribute to the kinetics, far-red light was used for photoexcitation and moreover the experiments were done in the presence of the PSII inhibitor DCMU. P700 photooxidation was recorded at different MV concentrations up to 2 mM (Fig. 4A). After an initial lag which is attributed to the presence of lumenal fast electron donors (plastocyanin/cytochrome c_6), the infrared signal rise due to $P700^+$ formation gets faster with the MV concentration. These measurements were made using sequential additions of MV with 15 min dark incubation after each addition. Control experiments were done in order to check that the changes in kinetics were not resulting from different dark incubation times (see Materials and methods). Due to the sigmoidal character of the kinetics, the data could not be simply fitted and the different kinetics were characterized by the time $t_{50\%}$ necessary for getting 50% of $P700^+$ formation. Fig. 4C describes the results of a control experiment where $t_{50\%}$ was measured upon the dark incubation time following a single addition of 0.25 mM MV. This shows that the MV effect is fully developed after 12 min, hence the dark incubation time that was used for measuring the [MV] dependence. This [MV] dependence is shown in Fig. 4B, from which one can deduce that the MV effect on P700 photooxidation saturates

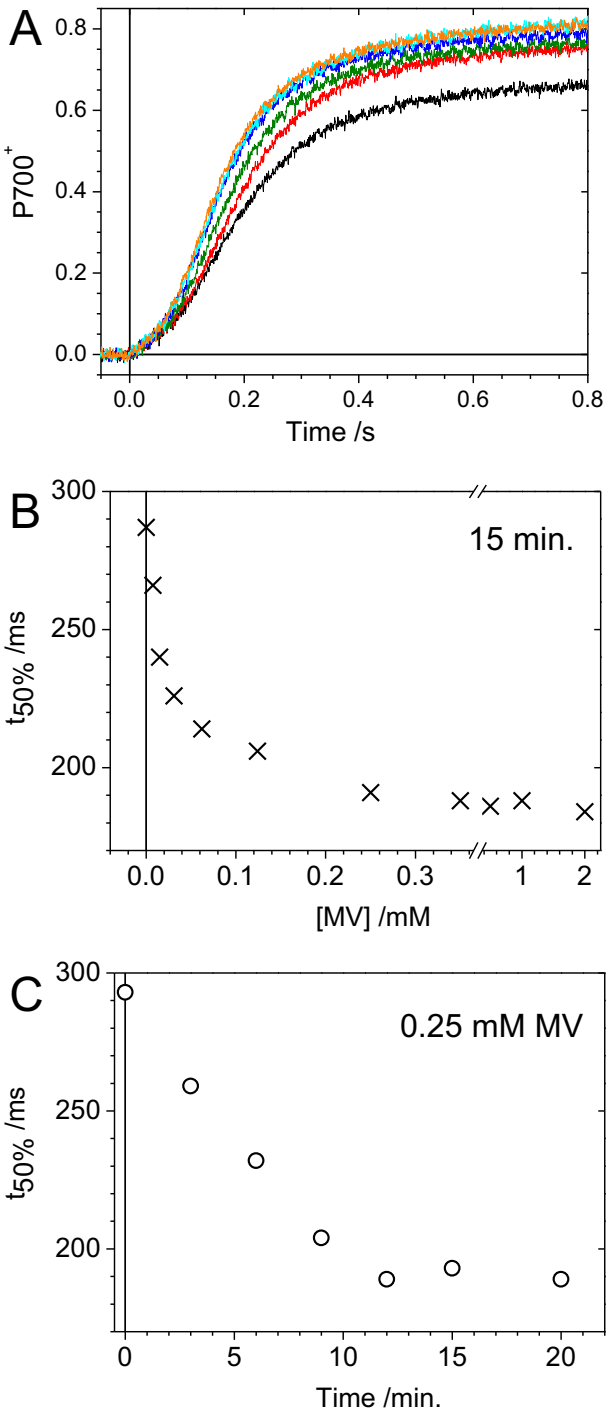

Fig. 4. *In vivo* P700 photooxidation at different MV concentrations and incubation times. *Synechocystis* cells at 10 μg chl/ml were studied in 1-cm cuvettes in the presence of 20 μM DCMU and at different MV concentrations (A and B) and incubation times (C). The sample was illuminated (from time 0) with far-red light (≥695 nm) at an intensity of 2.8 μmol photons $m^{-2}\ s^{-1}$. A. After each sequential MV addition, cells were incubated in darkness for 15 min. Each measurement is the average of 2 signals recorded at 15 and 17 min after MV addition. From the slowest to fastest rising kinetics: black (no MV), red (15 μM MV), green (62 μM), blue (250 μM), cyan (1 mM) and orange (2 mM). A value of 1 corresponds to the total $P700^+$ signal, which was measured at the end of the experiment with a far-red light intensity of 20 μmol photons $m^{-2}\ s^{-1}$ after addition of 40 μM of the cytochrome b_6f inhibitor 2,5-dibromo-6-isopropyl-3-methyl-1,4-benzoquinone (DBMIB). B. Time for 50% of P700 photooxidation, from kinetics shown in A. Note that the first concentration of MV shown here is 7.5 μM. C. Another sample was studied after a single addition of 0.25 mM MV. $t_{50\%}$ is shown as a function of the time of dark incubation following MV addition.

at a concentration of 0.25–0.35 mM. The effect observed here is attributed to the inhibition of recombination reactions between $P700^+$ and reduced acceptors $((F_A, F_B)^-$ as well as Fd_{red} populating $(F_A, F_B)^-$ by uphill ET). It led us to study NADPH formation *in vivo* at submillimolar MV concentrations, and more particularly at 0.3 mM.

3.5. Flash-induced NADPH formation in Synechocystis cells is weakly inhibited by MV below 1 mM

NADPH formation was recorded by fluorescence emission in a Dual-PAM spectrophotometer [39]. As previously reported, saturating 10 μs flashes elicit fast NADPH formation with half of signal rise observed at *c.* 8 ms after the flash [29]. This is shown in Fig. 5A before (trace a) and after (traces b to e) addition of 0.3 mM MV. Measurements with MV were recorded after 15 min of dark incubation following MV addition and were recorded sequentially as averages of 300 flashes. Whereas the first average gave a signal which is very similar to that in the absence of MV (b *vs* a), the final signal amplitude progressively decreased in the two next series (c and d). The last series (e) was recorded after continuous illumination of the cells for 45 s. The final signal amplitudes of these different traces are plotted in Fig. 5B (measured at 40–60 ms; black), in which results from similar experiments at larger MV concentrations are also shown (red and blue for 2 different experiments at [MV] = 1 mM, green for [MV] = 5 mM). The kinetics recorded at these MV concentrations are also shown in Supporting information (Fig. SI2). As extensive averaging is required for getting a sufficient-to-noise ratio, the plots in Fig. 5B are shown as horizontal bars figuring the extent of averaging. The levels plotted at the right of the vertical line correspond to signals measured after a single period of 45 s continuous illumination. From these data, it appears that the first series of kinetics after MV addition were almost not modified by the addition of 0.3 or 1 mM MV, whereas a 30% decrease in signal size was observed at 5 mM MV. The signal size decreased in the subsequent series of flashes with a much more rapid decrease with 5 mM MV, a concentration at which the signal almost disappeared after continuous illumination.

For MV concentrations ≤1 mM, these data are consistent with little or even no (for [MV] = 0.3 mM) reduction of MV that would compete after a flash for low potential electron carriers involved in NADPH formation ($(F_A, F_B)^-$, Fd_{red} or FNR_{sq}), in accordance with the *in vitro* results described above and with *in vivo* protein concentrations being in the submillimolar range (see Discussion). This statement is inferred from the first series of signals recorded after MV addition. For the next series, the signal decrease may be due to the effect of superoxide production mediated by little-efficient MV reduction. At higher MV concentration (5 mM), a competition by MV appeared to be significant from the beginning as seen from the first average after addition, although one cannot exclude that the first few flashes (not reliably observable due to a high noise level) might give a signal significantly larger than the average signal of the first 50 flashes.

3.6. MV oxidizes the NADP pool of Synechocystis cells in darkness

The effect of MV addition at low concentration (0.3 mM) was also studied by measuring NADPH formation under continuous illuminations of 2 s or 45 s durations (Fig. 6; same vertical scales for all parts; a level of 100 was arbitrarily set for the light-induced signal of trace b). Signals before MV addition (traces a and b) were first recorded as control experiments. Following the initial rise, a very small decrease (almost a plateau) is observed during the first few seconds of illumination. This is followed by a significant increase, which appears to be biphasic during a 45 s illumination (A). Such kinetic features (decrease/increase pattern in light) have been observed previously [28,29,39] and were tentatively interpreted as different steps limiting or activating the Calvin–Benson cycle (CBc) [28]. During the dark decay following a 2 s illumination, the signal decreases to a transient level below the baseline (trace b in B). This undershoot signal has been previously observed and

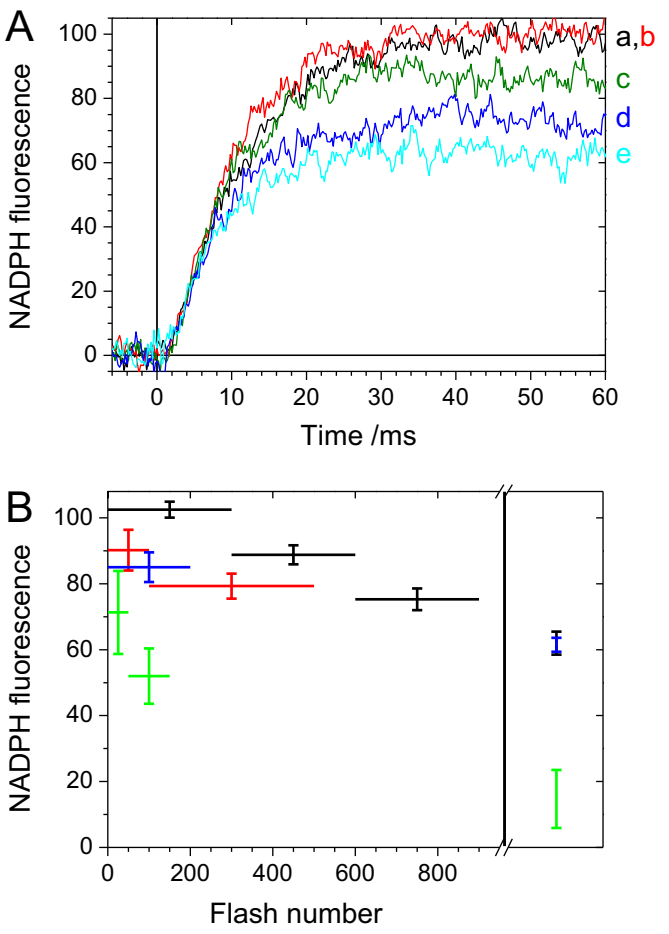

Fig. 5. *In vivo* flash-induced NADPH formation in the presence of methyl viologen. Fluorescence signals due to NADPH formation were measured in *Synechocystis* cells at 2.7 μg chl/ml ([PSI] = 29 nM). Signals were averaged both before (reference signal of 100) and after MV addition. After MV addition, the samples were incubated for 15 min in darkness before data acquisition. A. Fluorescence kinetics following 10 μs flashes. a: without MV; b to e, in the presence of 0.3 mM MV. After dark incubation in the presence of MV, kinetics from b to d were recorded sequentially. The sample was illuminated for 45 s before trace e was recorded. Experimental conditions: each trace corresponds to an average of 300 measurements, Δt = 4 s between two flashes. A signal of 100 corresponds to an apparent NADPH concentration of 20 nM (see Materials and methods). B. The size of the fluorescence signal of 4 different samples is plotted as a function of the flash number following MV addition (black: 0.3 mM, signals corresponding to data of part A; red and blue: 1 mM; green: 5 mM) and is normalized to the signal measured before MV addition (value of 100, at least 300 flashes were measured for each sample). For all signals left to the black vertical line, samples were illuminated only by 10 μs flashes after MV incubation whereas signals right to the line were recorded after one period of 45 s continuous illumination (averages of 100 to 400 flashes). For the left signals, the extent of signal averaging is indicated by the horizontal line. The signal levels were measured by fitting the fluorescence signal with a constant between 30 and 60 ms after the flash. The Y-error bars correspond to the noise level (standard deviation around the mean) and not to the standard error of the mean, which is 6 to 12 times smaller. All experiments were made once except for data in red which correspond to the average of 4 different samples.

was attributed to the activation of a NADPH-consumption process under light, presumably the CBc [28,29]. After addition of MV, the kinetics induced by a 2 s illumination (trace c) exhibit several features which are different from those without MV: firstly, the rising kinetics are initially slower in the presence of MV (during the first 150 ms of illumination) but the 2 kinetics cross at about 150 ms (C) with the final light signal with MV being larger than without it (B and C). Secondly, the decay with MV is faster than without it and moreover does not exhibit any undershoot (B and D).

The differences in signal levels observed for traces b and c under and after light can be easily understood if one assumes that the NADP pool is

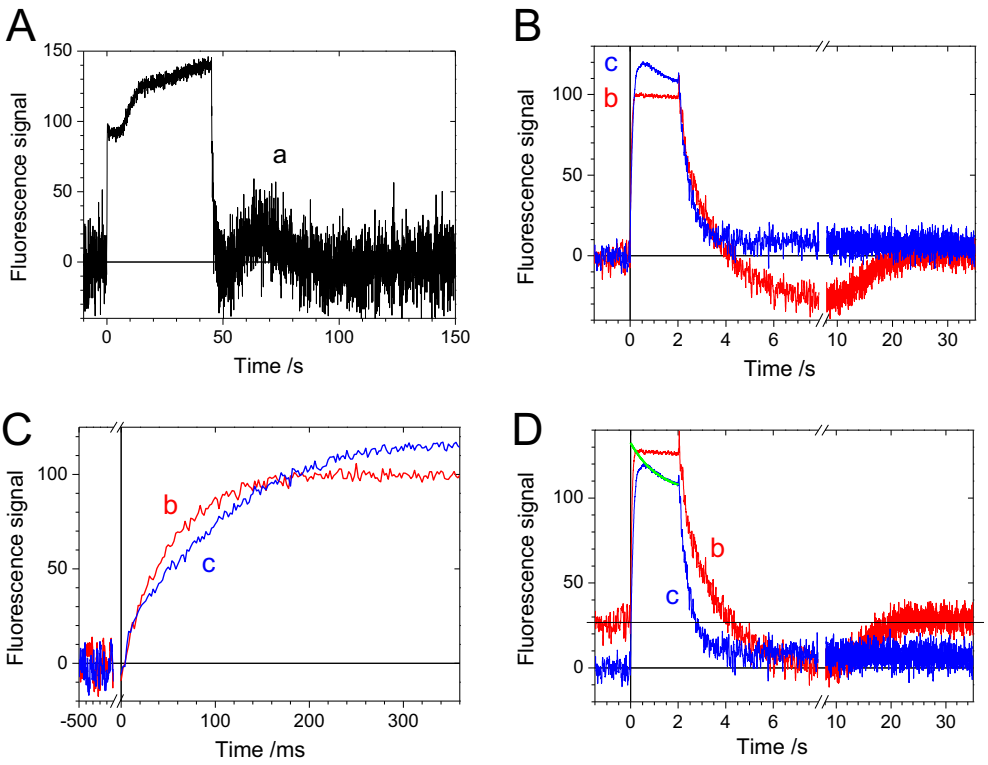

Fig. 6. *In vivo* light-induced NADPH formation in the presence of 0.3 mM MV. Fluorescence signals attributed to NADPH formation and decay were measured in *Synechocystis* cells at 2.7 μg chl/ml ([PSI] ≈ 29 nM). Actinic light intensity: 270 μmol photons m^{-2} s^{-1}. All parts of the figure were obtained with 2 different samples using an identical experimental protocol. Signals from both samples were very similar and were averaged. For each sample, measurements from a to c were recorded consecutively: initially, the cells contained no MV. After 2 preilluminations of 45 s (Δt = 4 min.), the signal induced by a 45 s illumination was recorded (a). 20 signals with 2 s illumination (Δt = 40 s) were averaged (b). A signal induced by a 45 s illumination was recorded with very similar kinetics to those of a (not shown). 0.3 mM MV was added and cells were incubated in darkness for 15 min before recording signals with 2 s illumination (c, average of 20 measurements, Δt = 40 s). In parts B, C and D, the same signals are shown with a shorter time scale in C or after vertical upshifting of b in D, so that the minimum signal level (at 8–10 s) was set to 0. For all other cases, the signal levels before illumination were set to 0. The under-light signal of c was fitted with a monoexponential decay between 0.7 and 2 s ($t_{1/2}$ = 0.85 s) and this decay was extrapolated to time 0 (smooth green line in D). Vertical scales of all parts are comparable with a scale of 100 arbitrarily set for the light-induced signal of trace b. This value of 100 corresponds to an apparent NADPH concentration of 121 nM (see Materials and methods).

completely oxidized in darkness in the presence of MV, whereas it is partly reduced in its absence. With this assumption, it becomes trivial that there is no undershoot with MV. It also easily explains why the light-induced signal is larger with MV, despite the fact that the rising kinetics are slower. In the absence of MV, it has been precedingly proposed that the undershoot level after CBc activation corresponds to full oxidation of the NADP pool [29]. This proposal was based on the observation that the signal decay after cessation of illumination is much faster than the signal increase following the undershoot. Although the duration of illumination is only 2 s in the present experiment (and therefore the light-activated decay is not yet at its maximum rate [29]), the minimum level may closely correspond to a fully oxidized pool as the decay is *c.* 4 times faster than the subsequent signal increase.

The idea that the NADP pool is fully oxidized on the one hand in darkness with MV and on the other hand only transiently after illumination without MV is supported by comparing the extent of signal changes under both conditions, as shown in part D: in this plot, trace b (no MV) was shifted upward so that the minimum level during the undershoot is set to zero whereas the fitted decay of the light signal with MV (trace c) was extrapolated to time 0 (green curve in D, see Figure legend). With such data treatment, the two maximum levels under light (green curve with MV at t = 0, plateau level without MV) are very similar (= 128–132 a.u.). This suggests that the same NADP (sub)pool (named rapid pool in the following) is observed ± MV, which is rapidly photo-reduced and rapidly reoxidized at cessation of illumination, with a level of dark-adapted reduction being different ± MV. That the NADP pool should be much more oxidized in darkness in the presence of MV is also supported by the 3-fold faster kinetics of after-light decay (from monoexponential fits of decay: $t_{1/2}$ = 0.94 and 0.29 s for traces b and c, respectively).

From trace a, it appears that, although a rise/decay pattern is present after the initial fast dark decay, there is no observable undershoot below the baseline. It should be also noted that the same kinetics as a were measured after recording b (data not shown), which allows decay kinetics of a and b to be reliably compared. The absence of undershoot may appear quite unexpected if it is interpreted as an incomplete reoxidation of the rapid pool (there is no reason why it should be incomplete after 45 s of illumination whereas it is complete after 2 s). However this can be easily explained if the signal is shifted upward because of another positive-going signal (*e.g.* secondary signal rise at t = 5–15 s in trace a) relaxing relatively slowly in darkness. In this interpretation, trace a exhibits an undershoot-like signal at t = 50–70 s corresponding to the rapid pool whereas the slow NAD(P)H decay at t > 70 s corresponds to that formed under light at t > 5 s.

3.7. MV at 0.3 mM partially inhibits NADPH formation during in vivo continuous illumination

Besides its effect on signal decay, MV influences the rising kinetics that are slower in its presence (c *vs* b in Fig. 6C). This cannot be explained by the sole increase in the decay rate (v_{decay_dark}) which is described in the above paragraph: if one assumes that, in the presence of MV, the rate of light-induced formation ($v_{formation\_light}$) is not modified whereas v_{decay_dark} increases, the stationary NADPH level under light should be reached faster with MV, contrary to what is observed. One can therefore conclude that $v_{formation\_light}$ decreases in the presence

of MV which can intercept electrons between PSI and $NADP^+$. This is opposite to the results of flash experiments, where no effect of addition at 0.3 mM MV was observed, at least for the first 300 flashes. In this context, it is worth mentioning the following control measurements: the average of the first 5 kinetics of 2 s illumination after MV addition gave the same kinetics, albeit with a larger noise, as those of trace c (which is an average of 50 measurements corresponding to 25 measurements per sample as data from 2 samples were averaged). Moreover, it was checked that the flash kinetics measured on the one hand before MV addition and on the other hand after a series of 10 continuous 2 s illuminations following addition of 0.3 mM MV were superimposable. These control measurements show that the difference in MV effect observed between flash and continuous light measurements is not a consequence of the accumulation of ROS species during continuous light.

It is also observed that the kinetics are similar ± MV up to *c.* 17 ms after the onset of illumination with an MV effect only visible at later times (Fig. SI3). At 17 ms, the signal amplitude of *c.* 27 a.u. (=33 nM of apparent NADPH in Fig. SI3, where the fluorescence signal is converted into apparent NADPH concentrations) corresponds to 1.65 times the signal measured after a flash (20 nM of apparent NADPH, see legends of Figs. 5 and 6), as if MV was becoming efficient after *c.* 1.5 to 2 PSI turnovers. It was also checked that increasing two-fold the actinic light intensity had no effect on the rising kinetics, both in the presence and absence of MV, as already reported in its absence [29].

The rate of MV reduction by stromal reductants can be crudely estimated from the difference in the kinetics ± MV that is clearly visible after 17 ms of illumination (Fig. SI3). At this time, the slope with MV is about half of its value without MV, which means that the instantaneous yield of NADPH formation is decreased two-fold by MV. From the slope decrease with MV, one can derive the "escape" rate of ET to MV per PSI from the knowledge of the concentrations of both light-induced NADPH and PSI (the possibility that this escape may occur *via* Fd_{red} is unimportant for this calculation). An approximate escape rate of 18 electrons per PSI per s was thus calculated, as detailed in Fig. SI3.

3.8. In vitro NADPH oxidation

We studied the oxidation of NADPH by MV in aerobic conditions in the presence of FNR and Fd (Fig. SI4). Although these results may appear somewhat trivial, they are reported to illustrate the different pathways which may be involved in NADPH oxidation by MV in cyanobacterial cells in darkness. These measurements show that neither MV nor Fd can react directly with NADPH, and that FNR is required for NADPH oxidation. A control measurement without MV also shows that FNR alone can slowly oxidize NADPH in the presence of oxygen. This oxidation is accelerated in the presence of MV and is further accelerated by the subsequent addition of Fd. Despite the large and unfavorable difference in midpoint potentials of the $NADP^+$/NADPH and MV^{+2}/MV^+ couples (−350 mV and −446 mV at pH 8, respectively; [3]), the continuous and prolonged oxidation of NADPH by MV observed in these experiments can be easily explained by the fact that MV^+ does not accumulate due to its fast reoxidation by oxygen.

4. Discussion

4.1. MV at submillimolar concentration is poorly efficient in intercepting electrons from PSI to $NADP^+$

From flash-induced kinetics of NADPH fluorescence, it appears that the yield of NADPH formation is only little decreased at MV concentrations of 0.3 and 1 mM, particularly when considering the first few hundreds of flashes following MV addition (Fig. 5). At 0.3 mM MV, there is even no observable signal change for the first 300 flashes. This somewhat unexpected behavior may be understood by considering on the one hand the *in vivo* concentrations of the protein partners involved in $NADP^+$ photoreduction and on the other hand the characteristics of MV reduction observed *in vitro* with purified cyanobacterial proteins: firstly, the approximate concentrations of Fd and FNR in the stromal space have been recently estimated in *Synechocystis* cells to be in the 100's μM range (600 ± 250 μM for Fd, 125 ± 40 for FNR; [44]). Secondly, from the flash-absorption data described in the present study, the inhibition of LET from PSI to $NADP^+$ by MV should be relatively inefficient, inasmuch as MV is not in large excess over the different proteins involved in $NADP^+$ photoreduction. This conclusion is made from the observation that the second-order rate constants of MV reduction (by the reduced PSI terminal acceptor, by Fd_{red} and by FNR_{sq}) are much smaller than the corresponding rate constants of the second-order processes involving the respective protein partners (Table 1): ratios between rate constants are thus found between 20 and 750.

Moreover the presence of PSI–Fd protein complexes, which can undergo submillisecond intracomplex ET [25,26], reduces the probability that MV can be reduced directly by PSI (Figs. 1 and 3). A situation where most of PSI is complexed with Fd may prevail *in vivo* in darkness for the following reasons: firstly, Fd has been found to be in (slight) excess over PSI [44]; secondly, the K_d of the PSI-Fd_{ox} complex (0.2–0.5 μM, [35,43]) is much larger than the Fd concentration *in vivo*; thirdly, Fd_{ox} has a much larger affinity for PSI than for all soluble partners where this affinity has been studied ($K_d \approx$ 6–8 μM μM for FNR_S, nitrate reductase and nitrite reductase [27,36,47]). After a flash, one can therefore expect that MV will compete with LET mostly at the level of Fd_{red}, after its dissociation from PSI. That the yield of NADPH formation after a flash is hardly affected shows that this competition is inefficient with Fd_{red} reacting with FNR_{Lox}/FNR_{Lsq} much faster than with MV.

4.2. MV is reduced by both Fd_{red} and $(F_A, F_B)^-$ when these species accumulate to significant stationary levels under continuous illumination

The situation under conditions of continuous illumination is different from that in flash experiments: the effect of MV addition at 0.3 mM becomes visible at 15–20 ms following the onset of illumination (Figs. 6C and SI3). This cannot be attributed to the blocking of LET by lack of terminal substrate, as a large part of NADP is still oxidized at this time. It must be due to PSI multiple turnover which allows accumulation of stromal reductants, namely $(F_A, F_B)^-$ and Fd_{red}, which are not consumed rapidly enough by FNR/NADP. This interpretation is in accordance with a previous experiment showing a significant decrease in the efficiency of NADPH formation (*vs* the amount of PSI charge separations) during a double flash experiment, when the two flashes are closely spaced so that they presumably lead to some transient accumulation of stromal reductants [29].

The present *in vitro* experiments show that Fd_{red} and $(F_A, F_B)^-$ reduce MV with similar rates, with Fd_{red} being slightly more reactive. Extrapolation to the *in vivo* situation can be reasonably made. This contrasts with the largely admitted view that MV accepts electrons from PSI, and not from Fd_{red}. It should be noted that this view is considered either as supported by the low midpoint potential of MV [2], or as self-evident (among many references, see [5,48]), or based on a misunderstood (and seemingly unread) publication of Fujii and coworkers [49] (among many references, see [7,11,14,50]). These authors [49] were studying the effect of $HgCl_2$, which destroys specifically F_B (*vs* F_A), both on the MV dependence of oxygen evolution by whole chloroplasts and on the MV inhibition of PSI recombination in PSI preparations. As indicated by the paper title, the authors were studying "the sites of electron donation of PSI to methyl viologen" and identified this site as being F_B. However by no means this paper can be taken as evidence that MV accepts electrons only from PSI *in vivo*, at the exclusion of Fd_{red}, and such a conclusion was indeed not derived by the authors.

The midpoint potential of (F_A, F_B) (−540 mV [51]) is much lower than that of MV (−446 mV [3]), contrary to that of Fd (−412 mV [46]), therefore favoring Trebst' hypothesis that MV accepts electrons from PSI [2]. The fact that the *in vitro* MV reduction by Fd_{red} is slightly

faster than MV reduction by $(F_A, F_B)^-$ means that the large difference in midpoint potentials is compensated by the interaction properties of MV with its protein partners. Electrostatic interactions are likely to be involved in this effect with MV being positively charged (+2 in the oxidized state) whereas Fd and the acceptor side of PSI (Fd docking region) are negatively [52] and positively charged [53], respectively. This could lead to longer-lived transient complexes of MV with Fd_{red} than with $(PSI\text{-}(F_A, F_B)^-)$ leading to more efficient MV reduction.

With regard to MV reduction by PSI, another difference between single flash experiments and continuous illumination should also be noticed: single turnover flashes will lead to a majority of PSI with F_A^- F_B, according to the generally accepted view that the midpoint potential of F_A is higher than that of F_B [51]. As F_B, which is the most accessible iron–sulfur cluster [22], is involved in MV reduction [49], this will affect the rate of MV reduction: $F_AF_B^-$ being in fast redox equilibrium with F_A^- F_B [20,21], the rate of MV reduction by PSI (as measured *in vitro* after a flash) will be the rate of MV reduction by $F_AF_B^-$ times the proportion of PSI with $F_AF_B^-$. The rate of MV reduction will therefore increase when both F_A and F_B are reduced, as it should occur in part of PSI under continuous illumination.

As an alternative explanation to the difference between MV reduction under continuous light and after a single turnover flash, a regulatory process may be triggered after a few photochemical turnovers and/or above a given level of NADP reduction (as seen in Figs. 6C and SI3 from the seemingly threshold effect in the MV inhibiting efficiency) which would increase the accessibility of the stromal reductants to MV by structural modifications. Such regulations involving disulfide reduction processes are well documented [54,55], but how they could operate and whether they could be fast enough to explain the present observations is not known.

4.3. Effect of MV addition in darkness

From the comparison of the dark NADPH decays following a short 2 s illumination ±0.3 mM MV (Fig. 6D), we proposed that most of the light-dependent NADP pool is oxidized in darkness in the presence of MV. This proposal is consistent with the observation that the after-light decay with MV (trace c in Fig. 6) is much faster than the NADPH formation which follows the signal undershoot (without MV) and which can be attributed to the oxidative pentose phosphate cycle (OPPc; see signal increase at 50–65 s in trace a of Fig. 6; see also Fig. 2B in [29]). Competition between dark formation by the OPPc and consumption by MV (+ other slower processes) would then lead to an almost fully oxidized NADP pool. *In vitro* consumption of NADPH in the absence of PSI (Fig. SI4) indicates that reduction of Fd by FNR coupled to oxidation of Fd_{red} by MV (reaction (5) in Fig. SI4B) may constitute the preferred pathway of NADPH consumption in *Synechocystis* cells in darkness although a NADPH-MV diaphorase activity of FNR can also contribute to this effect [56].

Oxidation of the NADPH pool by MV has been observed previously in animal cells (reviewed in [57]). Depletion of NADPH may contribute, together with the deleterious consequences of ROS production, to the high MV toxicity [57]. However MV-induced dark oxidation of NADPH in photosynthetic organisms has been previously observed only once, to our knowledge [58]. In this paper, no depletion of NADH was observed. These observations are consistent with the idea that dark NADPH depletion occurs mostly in chloroplasts with Fd being primarily involved in this process.

4.4. MV as a tool to inhibit PSI recombination reactions

Shortly after the onset of continuous illumination, the yield of MV reduction is close to that of NADPH formation, corresponding to a rate of *c.* 18 s^{-1} (Figs. 6C and SI3 for [MV] = 0.3 mM). In other words, in the presence of 0.3 mM MV, a concentration similar to those of the LET components, the yield of LET is *c.* 50% of its value in its absence (Fig. SI3, yield at 17 ms). The decrease in LET yield may be larger when the NADP pool becomes more reduced at later times, as suggested by the continuous decrease in the fluorescence level (Fig. 6D, t > 0.5 s, trace c). Is this level decreasing to zero during longer illumination (as being due to a large decrease in the LET yield) cannot be answered from the present data.

A rate of MV reduction of 18 s^{-1} is significantly faster than the recombination rate of 8 s^{-1} between $P700^+$ and $(F_A, F_B)^-$ that was measured *in vitro* [40]. As the intra-PSI recombination rate is not expected to be much different *in vivo*, one can conclude that MV at 0.3 mM efficiently suppresses PSI recombination reactions and *a fortiori*, the recombination reaction between $P700^+$ and Fd_{red} *via* uphill ET from Fd_{red} to (F_A, F_B). This statement is correct provided the light-induced formation of $(F_A, F_B)^-$ and Fd_{red} does not exceed MV reduction by these reductants. One can calculate an upper rate of the light-induced formation of stromal reductants from the rates of oxygen evolution: with a measured rate of 250 μmol O_2 mg^{-1} chl h^{-1} [29] consistent with previously measured values of 150–400 μmol O_2 mg^{-1} chl h^{-1} [59–62] and taking an *in vivo* ratio of 105 chlorophylls per PSI [29], the rate of formation of stromal reductants will correspond to 26 e^- per PSI per s. This suggests that under high light, recombination reactions will be greatly inhibited by 0.3 mM MV, even though larger MV concentrations may be necessary for full inhibition.

Efficient suppression of PSI recombination by MV is also consistent with the *in vivo* measurements of P700 photooxidation (Fig. 4), which also reveals that MV effects can be directly observed at concentrations less than 10 μM, in accordance with the numerous reports of MV sensitivity in the micromolar range (in cyanobacteria: [11,13,15,63,64]). It has been often argued that MV can fully inhibit CET [8,65–69]. This is probably the case if CET is measured as a slow (typically in the subsecond or second timerange) $P700^+$ reduction following continuous illumination. In the presence of MV, most stromal reductants will have been exhausted at the end of the illumination period and NADPH-dependent respiratory electron transfer will be slow. However, under experimental conditions where CET is relatively fast, as reported up to now only in the case of chloroplasts with rates in 10's of s^{-1} [66,70,71], CET may be only partially inhibited by MV at submillimolar concentrations, as is also the case for LET.

Acknowledgements

Dr. Bernard Lagoutte is deeply thanked for his gift of purified proteins, PSI, Fd and FNR_S. The author would like to thank Dr. Ghada Ajlani and Adrien Thurotte for their help in growing cultures and Dr. Anja Krieger–Liszkay for critical reading of the manuscript. This work was supported by a CEA/DSV "Bioénergie" grant and by the Agence Nationale de Recherche ANR-09-BLAN-0005-01.

Appendix A. Supplementary data

Supplementary data to this article can be found online at http://dx.doi.org/10.1016/j.bbabio.2014.10.008.

References

[1] A. Trebst, Inhibitors in electron flow: tools for the functional and structural localization of carriers and energy conservation sites, Methods Enzymol. 69 (1980) 675.
[2] A. Trebst, Measurement of hill reactions and photoreduction, Methods Enzymol. 24 (1972) 146–165.
[3] L. Michaelis, E.S. Hill, Potentiometric studies of semiquinones, J. Am. Chem. Soc. 55 (1933) 1481–1494.
[4] J.A. Farrington, M. Ebert, E.J. Land, K. Fletcher, Bipyridylium quaternary salts and related compounds. V. Pulse radiolysis studies of the reaction of paraquat radical with oxygen. Implications for the mode of action of bipyridyl herbicides, Biochim. Biophys. Acta 314 (1973) 372–381.
[5] C.F. Babbs, J.A. Pham, R.C. Coolbaugh, Lethal hydroxyl radical production in paraquat-treated plants, Plant Physiol. 90 (1989) 1267–1270.

[6] S.K. Herbert, G. Samson, D.C. Fork, D.E. Laudenbach, Characterization of damage to photosystems I and II in a cyanobacterium lacking detectable iron superoxide dismutase activity, Proc. Natl. Acad. Sci. U. S. A. 89 (1992) 8716–8720.
[7] D.J. Thomas, T.J. Avenson, J.B. Thomas, S.K. Herbert, A cyanobacterium lacking iron superoxide dismutase is sensitized to oxidative stress induced with methyl viologen but is not sensitized to oxidative stress induced with norflurazon, Plant Physiol. 116 (1998) 1593–1602.
[8] D.J. Thomas, J. Thomas, P.A. Youderian, S.K. Herbert, Photoinhibition and light-induced cyclic electron transport in ndhB$^-$ and psaE$^-$ mutants of *Synechocystis* sp PCC 6803, Plant Cell Physiol. 42 (2001) 803–812.
[9] M.M. Babykin, K.V. Sidoruk, V.V. Zinchenko, L.N. Nefedova, R. Gerff, S.V. Shestakov, On the involvement of the regulatory gene prqR in the development of resistance to methyl viologen in cyanobacterium *Synechocystis* sp PCC 6803, Russ. J. Genet. 39 (2003) 18–24.
[10] L.N. Nefedova, Y.S. Fantin, V.V. Zinchenko, M.M. Babykin, The prqA and mvrA genes encoding drug efflux proteins control resistance to methyl viologen in the cyanobacterium *Synechocystis* sp. PCC 6803, Russ. J. Genet. 39 (2003) 264–268.
[11] H. Maeda, Y. Sakuragi, D.A. Bryant, D. DellaPenna, Tocopherols protect *Synechocystis* sp. strain PCC 6803 from lipid peroxidation, Plant Physiol. 138 (2005) 1422–1435.
[12] J.C. Cameron, H.B. Pakrasi, Essential role of glutathione in acclimation to environmental and redox perturbations in the cyanobacterium *Synechocystis* sp. PCC 6803, Plant Physiol. 154 (2010) 1672–1685.
[13] P.S. Raghavan, H. Rajaram, S.K. Apte, Nitrogen status dependent oxidative stress tolerance conferred by overexpression of MnSOD and FeSOD proteins in *Anabaena* sp. strain PCC7120, Plant Mol. Biol. 77 (2011) 407–417.
[14] K. Hakkila, T. Antal, A.U. Rehman, J. Kurkela, H. Wada, I. Vass, E. Tyystjarvi, T. Tyystjarvi, Oxidative stress and photoinhibition can be separated in the cyanobacterium *Synechocystis* sp. PCC 6803, Biochim. Biophys. Acta 1837 (2014) 217–225.
[15] L.D. Moirangthem, S. Bhattacharya, K. Stensjo, P. Lindblad, J. Bhattacharya, A high constitutive catalase activity confers resistance to methyl viologen-promoted oxidative stress in a mutant of the cyanobacterium *Nostoc punctiforme* ATCC 29133, Appl. Microbiol. Biotechnol. 98 (2014) 3809–3818.
[16] M.A. Iannelli, F. Van Breusegem, M. Van Montagu, D. Inze, A. Massacci, Tolerance to low temperature and paraquat-mediated oxidative stress in two maize genotypes, J. Exp. Bot. 50 (1999) 523–532.
[17] T. Fujibe, H. Saji, K. Arakawa, N. Yabe, Y. Takeuchi, K.T. Yamamoto, A methyl viologen-resistant mutant of Arabidopsis, which is allelic to ozone-sensitive rcd1, is tolerant to supplemental ultraviolet-B irradiation, Plant Physiol. 134 (2004) 275–285.
[18] I. Murgia, D. Tarantino, C. Vannini, M. Bracale, S. Carravieri, C. Soave, *Arabidopsis thaliana* plants overexpressing thylakoidal ascorbate peroxidase show increased resistance to paraquat-induced photooxidative stress and to nitric oxide-induced cell death, Plant J. 38 (2004) 940–953.
[19] H. Jeon, Y.M. Jin, M.H. Choi, H. Lee, M. Kim, Chloroplast-targeted bacterial RecA proteins confer tolerance to chloroplast DNA damage by methyl viologen or UV-C radiation in tobacco (*Nicotiana tabacum*) plants, Physiol. Plant. 147 (2013) 218–233.
[20] K. Brettel, W. Leibl, Electron transfer in photosystem I, Biochim. Biophys. Acta 1507 (2001) 100–114.
[21] P. Sétif, Ferredoxin and flavodoxin reduction by photosystem I, Biochim. Biophys. Acta 1507 (2001) 161–179.
[22] P. Jordan, P. Fromme, H.T. Witt, O. Klukas, W. Saenger, N. Krauss, Three-dimensional structure of cyanobacterial photosystem I at 2.5 Å resolution, Nature 411 (2001) 909–917.
[23] Y. Mazor, D. Nataf, H. Toporik, N. Nelson, Crystal structures of virus-like photosystem I complexes from the mesophilic cyanobacterium *Synechocystis* PCC 6803, Elife 3 (2014) e01496.
[24] C.J. Batie, H. Kamin, Electron transfer by ferredoxin:NADP$^+$ reductase. Rapid-reaction evidence for participation of a ternary complex, J. Biol. Chem. 259 (1984) 11976–11985.
[25] P. Sétif, H. Bottin, Laser flash absorption spectroscopy study of ferredoxin reduction by photosystem I in *Synechocystis* sp. PCC 6803: evidence for submicrosecond and microsecond kinetics, Biochemistry 33 (1994) 8495–8504.
[26] P. Sétif, H. Bottin, Laser flash absorption spectroscopy study of ferredoxin reduction by photosystem I: spectral and kinetic evidence for the existence of several photosystem I-ferredoxin complexes, Biochemistry 34 (1995) 9059–9070.
[27] N. Cassan, B. Lagoutte, P. Sétif, Ferredoxin-NADP$^+$ reductase: kinetics of electron transfer, transient intermediates, and catalytic activities studied by flash-absorption spectroscopy with isolated photosystem I and ferredoxin, J. Biol. Chem. 280 (2005) 25960–25972.
[28] H.L. Mi, C. Klughammer, U. Schreiber, Light-induced dynamic changes of NADPH fluorescence in *Synechocystis* PCC 6803 and its ndhB-defective mutant M55, Plant Cell Physiol. 41 (2000) 1129–1135.
[29] J. Kauny, P. Sétif, NADPH fluorescence in the cyanobacterium *Synechocystis* sp. PCC 6803: a versatile probe for *in vivo* measurements of rates, yields and pools, Biochim. Biophys. Acta 1837 (2014) 792–801.
[30] B. Bouges-Bocquet, Electron and proton transfers from P-430 to ferredoxin-NADP-reductase in *Chlorella* cells, Biochim. Biophys. Acta 590 (1980) 223–233.
[31] A. Omairi-Nasser, A.G. de Gracia, G. Ajlani, A larger transcript is required for the synthesis of the smaller isoform of ferredoxin: NADP oxidoreductase, Mol. Microbiol. 81 (2011) 1178–1189.
[32] J.C. Thomas, B. Ughy, B. Lagoutte, G. Ajlani, A second isoform of the ferredoxin:NADP oxidoreductase generated by an in-frame initiation of translation, Proc. Natl. Acad. Sci. U. S. A. 103 (2006) 18368–18373.
[33] A. Korn, G. Ajlani, B. Lagoutte, A. Gall, P. Sétif, Ferredoxin:NADP$^+$ oxidoreductase association with phycocyanin modulates its properties, J. Biol. Chem. 284 (2009) 31789–31797.
[34] M. Rögner, P.J. Nixon, B.A. Diner, Purification and characterization of photosystem I and photosystem II core complexes from wild-type and phycocyanin-deficient strains of the cyanobacterium *Synechocystis* PCC 6803, J. Biol. Chem. 265 (1990) 6189–6196.
[35] P. Barth, I. Guillouard, P. Sétif, B. Lagoutte, Essential role of a single arginine of photosystem I in stabilizing the electron transfer complex with ferredoxin, J. Biol. Chem. 275 (2000) 7030–7036.
[36] P. Sétif, M. Hirasawa, N. Cassan, B. Lagoutte, J.N. Tripathy, D.B. Knaff, New insights into the catalytic cycle of plant nitrite reductase. Electron transfer kinetics and charge storage, Biochemistry 48 (2009) 2828–2838.
[37] R.J. Porra, W.A. Thompson, P.E. Kriedemann, Determination of accurate extinction coefficients and simultaneous equations for assaying chlorophylls *a* and *b* extracted with four different solvents: verification of the concentration of chlorophyll standards by atomic absorption spectroscopy, Biochim. Biophys. Acta 975 (1989) 384–394.
[38] C. Klughammer, U. Schreiber, Measuring P700 absorbance changes in the near infrared spectral region with a dual wavelength pulse modulation system, in: G. Garab (Ed.), Photosynthesis: Mechanisms and Effects, Photosynthesis: Mechanisms and Effects, vol. 5, Kluwer Acad. Publ, Netherlands, 1998, pp. 4357–4360.
[39] G. Schreiber, C. Klughammer, New NADPH/9-AA module for the DUAL-PAM-100: description, operation and examples of application, PAM Applic. Notes 2 (2009) 1–13.
[40] A. Diaz-Quintana, W. Leibl, H. Bottin, P. Sétif, Electron transfer in photosystem I reaction centers follows a linear pathway in which iron–sulfur cluster F_B is the immediate electron donor to soluble ferredoxin, Biochemistry 37 (1998) 3429–3439.
[41] B. Ke, The primary electron acceptor of photosystem I, Biochim. Biophys. Acta 301 (1973) 1–33.
[42] V. Fourmond, B. Lagoutte, P. Sétif, W. Leibl, C. Demaille, Electrochemical study of a reconstituted photosynthetic electron-transfer chain, J. Am. Chem. Soc. 129 (2007) 9201–9209.
[43] P. Barth, B. Lagoutte, P. Sétif, Ferredoxin reduction by photosystem I from *Synechocystis* sp. PCC 6803: toward an understanding of the respective roles of subunits PsaD and PsaE in ferredoxin binding, Biochemistry 37 (1998) 16233–16241.
[44] G. Moal, B. Lagoutte, Photo-induced electron transfer from photosystem I to NADP$^+$: characterization and tentative simulation of the *in vivo* environment, Biochim. Biophys. Acta 1817 (2012) 1635–1645.
[45] J.R. Bowyer, P. O'Neill, P. Camilleri, C.M. Todd, A study of the reaction between spinach ferredoxin and one-electron reduced herbicides of differing charge, Biochim. Biophys. Acta 932 (1988) 124–129.
[46] H. Bottin, B. Lagoutte, Ferredoxin and flavodoxin from the cyanobacterium *Synechocystis* sp. PCC 6803, Biochim. Biophys. Acta 1101 (1992) 48–56.
[47] A.P. Srivastava, M. Hirasawa, M. Bhalla, J.S. Chung, J.P. Allen, M.K. Johnson, J.N. Tripathy, L.M. Rubio, B. Vaccaro, S. Subramanian, E. Flores, M. Zabet-Moghaddam, K. Stitle, D.B. Knaff, Roles of four conserved basic amino acids in a ferredoxin-dependent cyanobacterial nitrate reductase, Biochemistry 52 (2013) 4343–4353.
[48] G. Schansker, S.Z. Toth, R.J. Strasser, Methylviologen and dibromothymoquinone treatments of pea leaves reveal the role of photosystem I in the Chl *a* fluorescence rise OJIP, Biochim. Biophys. Acta 1706 (2005) 250–261.
[49] T. Fujii, E. Yokoyama, K. Inoue, H. Sakurai, The sites of electron donation of photosystem I to methyl viologen, Biochim. Biophys. Acta 1015 (1990) 41–48.
[50] G. Varadi, E. Darko, E. Lehoczki, Changes in the xanthophyll cycle and fluorescence quenching indicate light-dependent early events in the action of paraquat and the mechanism of resistance to paraquat in *Erigeron canadensis* (L.) Cronq, Plant Physiol. 123 (2000) 1459–1469.
[51] K. Brettel, Electron transfer and arrangement of the redox cofactors in photosystem I, Biochim. Biophys. Acta 1318 (1997) 322–373.
[52] K. Fukuyama, Structure and function of plant-type ferredoxins, Photosynth. Res. 81 (2004) 289–301.
[53] P. Sétif, N. Fischer, B. Lagoutte, H. Bottin, J.D. Rochaix, The ferredoxin docking site of photosystem I, Biochim. Biophys. Acta 1555 (2002) 204–209.
[54] M. Lindahl, T. Kieselbach, Disulphide proteomes and interactions with thioredoxin on the track towards understanding redox regulation in chloroplasts and cyanobacteria, J. Proteomics 72 (2009) 416–438.
[55] K.J. Dietz, Peroxiredoxins in plants and cyanobacteria, Antioxid. Redox Signal. 15 (2011) 1129–1159.
[56] M.G. Mediavilla, G.A. Di Venanzio, E.E. Guibert, C. Tiribelli, Heterologous ferredoxin reductase and flavodoxin protect Cos-7 cells from oxidative stress, PLoS ONE 5 (2010) e13501.
[57] J.S. Bus, J.E. Gibson, Paraquat — model for oxidant-initiated toxicity, Environ. Health Perspect. 55 (1984) 37–46.
[58] I. Iturbe-Ormaetxe, P.R. Escuredo, C. Arrese-Igor, M. Becana, Oxidative damage in pea plants exposed to water deficit or paraquat, Plant Physiol. 116 (1998) 173–181.
[59] J.J. Benschop, M.R. Badger, G.D. Price, Characterisation of CO_2 and HCO_3^- uptake in the cyanobacterium *Synechocystis* sp. PCC6803, Photosynth. Res. 77 (2003) 117–126.
[60] W. Majeed, Y. Zhang, Y. Xue, S. Ranade, R.N. Blue, Q. Wang, Q.F. He, RpaA regulates the accumulation of monomeric photosystem I and PsbA under high light conditions in *Synechocystis* sp. PCC 6803, PLoS ONE 7 (2012) e45139.
[61] T. Wallner, Y. Hagiwara, G. Bernat, R. Sobotka, E.J. Reijerse, N. Frankenberg-Dinkel, A. Wilde, Inactivation of the conserved open reading frame ycf34 of *Synechocystis* sp. PCC 6803 interferes with the photosynthetic electron transport chain, Biochim. Biophys. Acta 1817 (2012) 2016–2026.
[62] Q.J. Wang, A. Singh, H. Li, L. Nedbal, L.A. Sherman, Govindjee, J. Whitmarsh, Net light-induced oxygen evolution in photosystem I deletion mutants of the cyanobacterium *Synechocystis* sp. PCC 6803, Biochim. Biophys. Acta 1817 (2012) 792–801.

[63] K. Kojima, T. Suzuki-Maenaka, T. Kikuchi, H. Nakamoto, Roles of the cyanobacterial isiABC operon in protection from oxidative and heat stresses, Physiol. Plant. 128 (2006) 507–519.
[64] N. Blot, D. Mella-Flores, C. Six, G. Le Corguille, C. Boutte, A. Peyrat, A. Monnier, M. Ratin, P. Gourvil, D.A. Campbell, L. Garczarek, Light history influences the response of the marine cyanobacterium *Synechococcus* sp. WH7803 to oxidative stress, Plant Physiol. 156 (2011) 1934–1954.
[65] G. Cornic, N.G. Bukhov, C. Wiese, R. Bligny, U. Heber, Flexible coupling between light-dependent electron and vectorial proton transport in illuminated leaves of C_3 plants. Role of photosystem I-dependent proton pumping, Planta 210 (2000) 468–477.
[66] P. Joliot, A. Joliot, Cyclic electron transfer in plant leaf, Proc. Natl. Acad. Sci. U. S. A. 99 (2002) 10209–10214.
[67] P. Joliot, A. Joliot, Quantification of cyclic and linear flows in plants, Proc. Natl. Acad. Sci. U. S. A. 102 (2005) 4913–4918.
[68] F. Li, Q.Y. Wu, Y.L. Sun, L.Y. Wang, X.H. Yang, Q.W. Meng, Overexpression of chloroplastic monodehydroascorbate reductase enhanced tolerance to temperature and methyl viologen-mediated oxidative stresses, Physiol. Plant. 139 (2010) 421–434.
[69] P. Joliot, G.N. Johnson, Regulation of cyclic and linear electron flow in higher plants, Proc. Natl. Acad. Sci. U. S. A. 108 (2011) 13317–13322.
[70] P. Joliot, D. Béal, A. Joliot, Cyclic electron flow under saturating excitation of dark-adapted *Arabidopsis* leaves, Biochim. Biophys. Acta 1656 (2004) 166–176.
[71] J. Alric, Redox and ATP control of photosynthetic cyclic electron flow in *Chlamydomonas reinhardtii* (II) involvement of the PGR5-PGRL1 pathway under anaerobic conditions, Biochim. Biophys. Acta 1837 (2014) 825–834.